Check for updates

Geochemical cycles of arsenic in historic tin tailings from multiple ore sources: an example from Australia

Amelia Corzo Remigio [iD] **· David A. Rubinos ·**
Antony van der Ent · Mansour Edraki

Abstract In this work, we studied a geochemically unique abandoned tin mining tailings facility in tropical north Queensland, Australia. Tin mining residues from local operations were reprocessed and left without proper remediation, after which native plant species colonised this site over time. The aim of this study was to characterize the mine tailings to understand the geochemistry and predict the potential mobility and bioavailability of major contaminants, arsenic and tin. Major and trace minerals were identified with X-ray diffraction (XRD) and scanning electron microscopy with energy-dispersive X-ray spectroscopy (SEM-EDS). Acid digestion and sequential extraction procedures were used to quantify elemental concentrations and potential mobility. We found that the highly oxidized tailing cells were dominated by quartz with limited buffering capacity to prevent acid mine drainage formation, consequently creating an acidic environment (pH 4). Arsenic (As) and tin (Sn) were identified as the main contaminants in the tailings with concentrations of up to 2980 µg g^{-1} and 2910 µg g^{-1}, respectively. Tin was mainly bound to the residual fraction (52% of total Sn) and crystalline Fe-oxide fraction (33% of total Sn), limiting its release and mobility. The bulk of As (~77% of total As) was present in the crystalline Fe-oxide fraction, while ~19% in the amorphous/poorly crystalline Fe-oxide fraction. The bioavailable As fraction was negligible (~1%), and this was confirmed by limited As accumulation in terrestrial and aquatic plants (*Cyperaceae* sp., *Eleocharis equisetina*, and *Poaceae* sp.) sampled at the site. This interdisciplinary study reveals biogeochemical properties of Sn tailings, the fate of As, and how native plants can thrive in this unfavourable environment. This information can potentially guide further phytostabilization efforts at this site.

A. Corzo Remigio (✉) · A. van der Ent · M. Edraki
Centre for Mined Land Rehabilitation, Sustainable Minerals Institute, The University of Queensland, Brisbane, Australia
e-mail: amelia.corzoremigio@uq.edu.au

D. A. Rubinos
International Centre of Excellence Chile, Sustainable Minerals Institute, The University of Queensland, Brisbane, Australia

1 Introduction

Mining activities generate large amounts of residues, as typically only 1–5% of the material processed is ore of economic value (Edraki et al., 2014; Lottermoser, 2010a). Before enforcement of environmental laws, mine wastes were often left without appropriate remediation and management (Folguera et al., 2016).

Historical mining liabilities are consequently widespread worldwide (Candeias et al., 2019; Coelho et al., 2011). Sulfide minerals are an ubiquitous part of many geological complexes and mine waste storage facilities, and when exposed to the atmosphere, oxidise and produce acid mine drainage (AMD), which can potentially mobilise toxic metals and metalloids (Dold, 2014; Lottermoser, 2010b; Nordstrom et al., 2015). If not contained, the metal(loid)s release can surpass spatial and time boundaries, ultimately threatening human health and ecosystems (Olías et al., 2006). Therefore, detailed characterization of mining waste liabilities is fundamental to predict pollution potential of metal(loid)s and to prioritize appropriate remediation measures.

After mineral processing, the residual minerals deposited within the tailings are known as primary minerals, and the minerals that are formed through *in situ* weathering are known as secondary minerals (Jambor, 2003). Pyrite (FeS_2) is one of the most abundant, non-valuable sulfides (Vaughan, 2006), and one of the main AMD producers (Lottermoser, 2010b). The fate of metal(loid)s depends on the mineralogy of the waste material; if carbonate minerals are present in substantial quantities, they can buffer against acid mine drainage production (Dold, 2014; Jambor, 2003). Furthermore, the formation of secondary minerals under natural weathering can attenuate the release of toxic pollutants; for example, part of the As released from arsenopyrite (the primary mineral of As) is retained as secondary products, *i.e.* scorodite ($FeAsO_4 \cdot 2H_2O$), amorphous ferric arsenate ($FeAsO_4$), and Fe^{III} oxyhydroxides (Murciego et al., 2011; Paktunc et al., 2004). Of all of these secondary minerals, scorodite is the most common (Craw & Bowell, 2014), whilst Fe^{III} oxyhydroxides contains up to 22% As (Paktunc et al., 2004).

Phytostabilization is a cost-effective and ecologically favourable method that limits the translocation of metal(loid)s to the aerial tissues of plants, thereby preventing food-chain bioaccumulation and biomagnification (Chaney & Baklanov, 2017). Plants have evolved different mechanisms for metal(loid) tolerance, and based on their uptake can be classified either as *hyperaccumulators*, *indicators*, or *excluders* (Baker, 1981, 1987). Hyperaccumulators concentrate extraordinarily high levels of metal(loid)s in their above-ground tissues, whilst indicators accumulate metal(loid)s in accordance to the bioavailability in the soil, whereas excluders maintain low

metal(loid) concentrations in the shoots in response to high soil exposure. This last category of plants is most suitable for phytostabilization. For example, the native Australian plants *Bothriochloa macra* (Poaceae) and *Enteropogon acicularis* (Poaceae) only attain 1.1–1.4 µg As g^{-1} in their leaves when growing in As-rich sulfidic gold mine tailings with 2806 µg As g^{-1} (Doronila et al., 2014). *Eucalyptus* sp. has been reported to accumulate 3.1–5.6 µg As g^{-1} in their shoots when growing in amended As-rich gold mine tailings with As concentrations between 1000–2000 µg As g^{-1} (Sanchez-Palacios et al., 2013). In 85-year-old As-rich tin tailings in Tasmania, the Australian native species, *Acacia dealbata* (Fabaceae), *Lomandra longifolia* (Asparagaceae), *and Poa labillardieri* (Poaceae), were grown in amended tailings and proved to have potential for vegetative establishment at the site (Macdonald et al., 2017).

Historic mining in Australia dates back to more than 200 years, and the absence of adequate regulation resulted in more than 80 000 abandoned mines (Minerals Council of Australia, 2017; Unger et al., 2012; Werner et al., 2020). Some of these liabilities were studied because of the toxicological effects of abandoned mines with high content of As, such as in Victoria (Pearce et al., 2012), New South Wales (Ashley & Lottermoser, 1999; Telford et al., 2009), and Queensland (Matanitobua et al., 2007; Noller et al., 2012). The Jumna tailings facility, located in north Queensland, has been of interest due to the reported high concentrations of As (up to 593 µg g^{-1}) in the tailings (Lottermoser & Ashley, 2006, 2011). The main processed mineral at Jumna was the oxide cassiterite (SnO_2), although sulfides were also identified in this polymetallic processing site (Garrad & Bultitude, 1999).

The geochemical characterization of toxic elements has been extensively studied in gold (Au) mine waste (Blowes et al., 1998), nickel (Ni), and base metals wastes (Rodríguez-Hernández et al., 2021; Sidenko et al., 2007). Nonetheless, only a limited number of studies addressed As mobilisation in cassiterite mine tailings (Gault et al., 2005; Hebbard et al., 2017; Noble et al., 2016; Romero et al., 2014). Even less is known about Sn mobilisation and fate in the environment (Haase et al., 2021). Therefore, the aim of this research was to characterize the Jumna tailings in relation to its geochemistry, the mobilisation of main pollutants, and their bioavailability to plants, with an emphasis on As and Sn. The tailings were studied for their geochemical and mineralogical characteristics, coupled with chemical

fractionation and bioavailability for plants of the target elements. X-ray diffraction (XRD) was used to identify minerals, whilst scanning electron microscopy with energy-dispersive X-ray spectroscopy (SEM - EDS) were used to detect trace and secondary minerals in the tailings. A sequential extraction procedure (SEP) was used to study the geochemical distribution of As and to estimate its potential mobilisation and bioavailability. For this purpose, samples of plants growing in the tailings were collected and characterised for their metal(loid) concentrations. Finally, a metal(loid) enrichment ratio analysis was performed to draw overall conclusions of the contamination status of the Jumna facility. This is the first study addressing the fractionation and fate of As and other inorganic pollutants in this tin tailing–native Australian flora system.
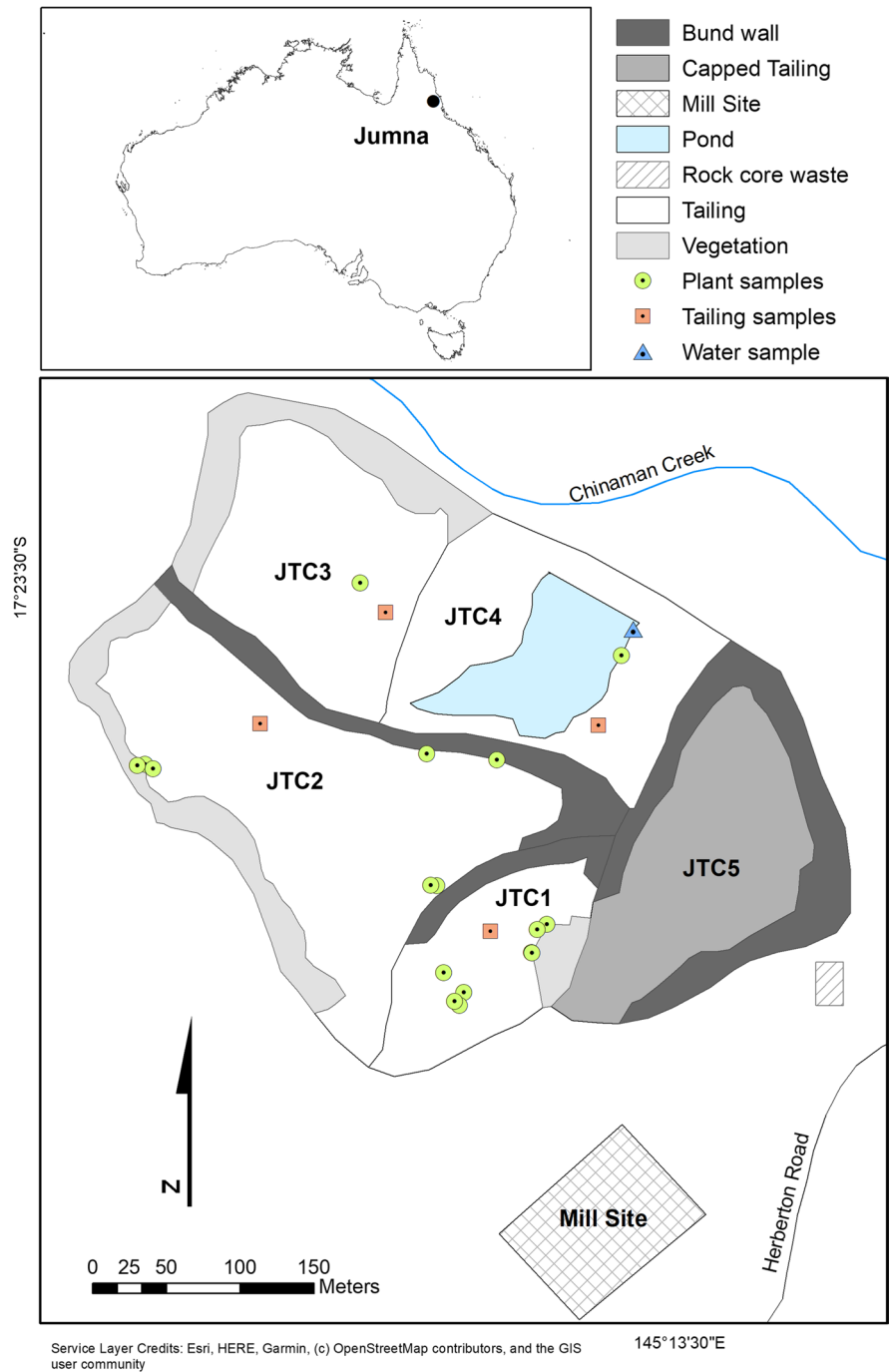
2 Materials and Methods

2.1 Site Description

The Jumna tailing storage facility is located near Irvinebank in far north Queensland, Australia, at 17°23.64′S, 145°13.42′E (Fig. 1), with a local climate that is tropical with an annual average rainfall of 1198 mm (Bureau of Meterorology, 2020). The discovery and exploitation history of tin deposits in Irvinebank and the surrounding areas dates back to 1880s–1980s. The mineralization in this area originates from the Late Carboniferous and consists of cassiterite and sulfides (pyrite, chalcopyrite, galena, and arsenopyrite) in a gangue of quartz, tourmaline, chlorite, garnet, and kaolite (Dash et al., 1991). The Jumna Mill operated from 1972 to 1989 and treated waste material, tailings, and hard rock tin ores from the Irvinebank deposits (Lottermoser & Ashley, 2006). The process of separation involved crushing, grinding, and gravimetric sorting to concentrate cassiterite. Approximately 0.15 Mt tailings (Garrad & Bultitude, 1999) were disposed in five different cells JTC1, JTC2, JTC3, JTC4, and JTC5 (in total covering ~0.06 km^2), located adjacent to Chinaman Creek (Fig. 1) (Lottermoser & Ashley, 2006). As the tailings were left uncovered, they were subjected to sulfide oxidation, AMD formation, leaching, and erosion (Lottermoser & Ashley, 2006). Due to these processes, the JTC4 cell was permanently covered with wastewater coming from JTC5 seepage.

In 1997, rehabilitation trials were conducted on the JTC5 cell by seeding with grasses, and preventing seepage leaking into the Chinaman creek using a geomembrane liner (Lottermoser & Ashley, 2011). To this day, the other cells at this site (JTC1, JTC2, JTC3, and JTC4 cells) remain exposed to the environment, although plants have now advantageously colonised certain areas.

2.2 Field Sampling

Initial composite samples from the four cells (JTC1, JTC2, JTC3, and JTC4) were received in late 2018. These samples were characterised in the Environmental Geochemistry Laboratory, The University of Queensland and the analysis of major elements yielded on average a composition of 66% of SiO_2, 13% of Al_2O_3, 11% Fe_2O_3, 0.1% CaO, and the trace metal(loid) s concentrations were: 1240 μg As g^{-1}, 472 μg Zn g^{-1}, 471 μg Pb g^{-1}, 419 μg Cu g^{-1}, and 397 μg Sn g^{-1}. Using this information, a fieldtrip was undertaken to more systematically collect samples from tailing profiles, from waters, and from the local plant vegetation (Fig. 1). The fieldwork was conducted during the dry season in October 2019. The tailing profile samples (collected from 0–1.4 m depth) and the plant substrate samples (collected from 0–20 cm depth) were oven-dried at 40°C for 48 h, homogenised, sieved to < 2 mm, and 5–10 g then pulverised (< 63 μm) in an agate ball mill. Measurements of the pH and electrical conductivity (EC) (25°C) were performed in a 1:5 tailing/water mixture (Rayment et al., 2011). A water sample was collected in an acid-washed low-density polyethylene bottle from the pond at JTC4, stored in an Esky with ice and submitted for immediate analysis to the Environmental Geochemistry Laboratory at UQ. Physico-chemical parameters, *i.e.* pH, oxidation-reduction potential (ORP), and EC, were measured in the field with a Sension$^+$ MM150 DL portable multi-parameter instrument. Plant samples were thoroughly washed with deionised water (DI), desegregated (shoots and roots), and oven-dried at 40°C for 72 h. An aliquot of the biomass was ground in a batch mill tube, IKA Tube Mill 100 Control. Pictures of plants were taken for identification through comparison with Queensland flora books (Brock, 1993; Milson, 2000) and further validation with a botanist with expertise in the Australian tropical flora.

Fig. 1 Location map of Jumna facility and sampling points of plants, tailings, and water

Service Layer Credits: Esri, HERE, Garmin, (c) OpenStreetMap contributors, and the GIS user community

2.3 X-ray Diffraction (XRD)

Powder aliquots (< 63 μm) of the composite tailing samples from the JTC1, JTC2, JTC3, and JTC4 cells sampled in 2018 were submitted for quantitative XRD mineralogical analysis at the Sietronics Laboratory, Canberra, Australia. A Bruker-AXS D2 XRD instrument with a copper target was operated at 30 kV and 10mA, and the data was recorded over a range of 3 to 70°2θ, with a 0.02-degree step and 2 s per step count time. The Bruker DIFFRAC.EVA Search/Match software and ICDD PDF-2 database were used to identify the phases

and SIROQUANTTM version 4 software quantified the mineral proportion. Furthermore, two sub-samples from the tailing profile JTC3 were submitted for XRD analysis at the Queensland University of Technology Central Analytical Research Facility, Brisbane, Australia. A PANalytical X'Pert Pro powder diffractometer with a cobalt target was used. JADE (V2010), Materials Data Inc., EVA (V5, Bruker), and X'Pert Highscore Plus (V4, PANalytical) with PDF4+, AMCSD, and COD databases were used to identify the phases. The addition of corundum (Al_2O_3) as an internal standard (20 wt%) facilitated the quantification of mineral abundances of the identified phases in the JTC3 sub-samples.

2.4 Scanning Electron Microscopy and Energy-Dispersive X-ray Spectroscopy (SEM-EDS)

Two sub-samples from cell JTC3 were sent to Laboratory at the School of Earth and Environmental Science (SEES) at The University of Queensland for preparation of polished blocks (25 mm diameter × 10 mm thick). Polished sections were sputter-coated with carbon (~25 nm) and mounted on stubs. The samples were imaged using a scanning electron microscope in back-scattered electron mode for energy-dispersive X-ray spectroscopy analysis on a Hitachi SU3500 instrument equipped with a 50 mm^2 Oxford Instruments silicon drift detector. Analyses were made at 100–1000× magnification at 5–15 kV with lower accelerator energies for imaging with secondary electron returns only, and higher accelerator energies for imaging in back-scatter mode and for the EDS point analyses. Count rates were 10 000–25 000 cps and the data were analysed using AZtecEnergy Microanalysis software with C K-line and O K-line included and considering the carbon coating.

2.5 Elemental Analysis

For tailings and plant substrate analysis, dried and pulverised samples were weighed to 100 mg, and poured into quartz tubes to which reverse aqua regia: 5 mL of HNO_3 (70%) and 2 mL of HCl (37%) was added. The digestion was performed using a ColdBlock SB15S Digester during four rounds of 240 s each (totalling 16 min). The ColdBlock system uses focused infrared radiation to speed the sample breakdown and a cooling system to regulate the temperature (Wang et al., 2014). Samples were then brought to volume (40 mL) with

ultrapure water (Millipore, resistivity = 18.2 MΩ·cm^{-1} at 25°C) before analysis by inductively coupled plasma atomic emission spectrometry (ICP-AES) as described below. For plant analysis, ground and dried biomass were weighed up to 100 mg, or less depending on the total weight of the sample, in 10 mL polypropylene tubes, and then pre-digested using 2 mL HNO_3 (70%) for 24 h, then digested using a hot block (Thermo Scientific Digital Dry Bath) for 1 h at 70 °C, and then at 125°C for another hour. Digested samples were brought to volume (10 mL) with ultrapure water (Millipore, resistivity = 18.2 MΩ·cm^{-1} at 25°C). The analysis of the samples was conducted by ICP-AES in a Thermo Scientific iCAP 7400 instrument for major elements (Fe, Al, Ca, K, Mn, Mg, Na, P) and trace elements (Cu, Zn, Pb, As, Sn) in radial and axial modes depending on the element and concentration. All elements were calibrated with a 4-point curve covering analyte ranges in the samples. In-line internal addition standardization using yttrium was used to compensate for matrix-based effects. Quality controls included matrix blanks, certified reference material (Sigma-Aldrich Periodic table mix 1 for ICP TraceCERT®, 33 elements, 10 mg L^{-1} in HNO_3), and Standard Reference Material (NIST Estuarine Sediment 1616 and NIST Apple 1515). Instrument parameters were RF power of 1150 W, auxiliary gas flow of 0.5 L min^{-1}, coolant gas flow of 12 L min^{-1}, nebuliser gas flow L min^{-1}, nebuliser gas pressure of 220 kPa, and a pump speed of 50 rpm.

2.6 Sequential Extraction Procedure (SEP)

This method entails subjecting a solid sample to a series of different successive chemical extractions with solutions of progressively stronger action to selectively remove or dissolve a specific form or solid component that the element of interest is associated with (Hall et al., 1996; Hass & Fine, 2010). Since the Jumna tailings are mostly enriched in As, the applied SEP protocol has been designed to study the partitioning of this metalloid in tailings. Arsenic is different compared to cationic metals in that it exhibits anionic behaviour in aqueous systems, which generally makes it more mobile than metals in their cationic form (Brand-stetter et al., 2000). Hence, three schemes were tailored for this protocol, which involved seven extraction steps (Supplementary Table S1), the first was proposed for metal(loid)s in mine waste (Dold,

2003), whilst the second and third were specifically designed for As (Keon et al., 2001; Lombi et al., 2000). After each extraction step, the suspensions were centrifuged, filtered, and analysed for major, minor, and trace elements as described in the "*Elemental Analysis*" section. Two profile samples from JTC3 were used for the SEP, with six replicates used for each method.

2.7 Metal(loid) Enrichment Ratio

In order to estimate the degree of contamination and anthropogenic disturbance on the study area, the enrichment ratio (ER) was used. This ratio uses a pre-industrial reference value to compare with and provides a precise scale, although natural geochemical processes are not considered (Kowalska et al., 2018). The enrichment ratio (ER) is a pollution ranking system to categorize the degree of pollution (Sutherland, 2000). It is based on the following equation:

$$ER_n = \frac{\left[\frac{C_n\ Sample}{C_{Fe}\ Sample}\right]}{\left[\frac{BE_n Background}{BE_{Fe} Background}\right]}$$

where C_n is the concentration of the element n in the sample, C_{Fe} is the concentration of iron (Fe) in the sample, BE_n is the background concentration of the element n, and BE_{Fe} is the background concentration of Fe. The geochemical background concentration used was selected from the Australian geochemical survey, from the nearest top local catchment, Cairns, QLD (16°51′25.2″S, 145°42′54″E), outlet sediment (0–10 cm), fraction (<2 mm size) (Cooper et al., 2010; de Caritat & Cooper, 2011). The background for Fe was selected as a comparative element due to its abundance in Jumna tailings, criteria also used in a previous study (White & Tittlebaum, 1985). The degree of pollution has been categorized in five classes based on ER: ER < 2 minimal pollution, $2 \leq ER \leq 5$ moderate pollution, $5 \leq ER \leq 20$ significant pollution, $20 \leq ER \leq 40$ very strong pollution, and > 40 extreme pollution (Sutherland, 2000). While this index helps to understand the element enrichment of tailings, it is fundamental to note that metal(loid)s are contained within the facility and it is not measured downstream in natural soils.

3 Results

3.1 Tailings

The XRD and SEM-EDS results are presented in Supplementary Table S2 and S3, while Table 1 shows the elemental analysis of tailing samples, and Supplementary Table S5 shows that of water. The uncapped tailings cells are highly oxidized (Fig. 2) and only the JTC4 has an unoxidized zone at the bottom (Fig. 2d), which reflects the original sulfide tailing composition. Cemented and hardpan layers were observed (Fig. 2a, b) in the surface of JTC1, JTC2, and JTC3 cells, which were formed by precipitation and dehydration of secondary phases as amorphous, poorly crystalline, and well-crystallised minerals, studied at Jumna in detail by Lottermoser and Ashley (2006). A water body covers partially JTC4, and efflorescences are visible on the surface, *i.e.* $CuSO_4$ (Fig. 2c). In cells JTC1 to JTC4, quartz is the major mineral in tailings, followed in abundance by chlorite, kaolinite, muscovite, albite, and orthoclase (Supplementary Table S2). The JTC4 tailings with less content of quartz differ from the other cells and present minor quantities of jarosite and hematite. The mineralogy of profile samples of cell JTC3 showed that the JTC3-1 (0–30 cm) and JTC3-2 (30–130 cm) zones are similar with dominance of quartz and less percentage of illite/mica, schrol, plagioclase, goethite, and cassiterite, while the amorphous proportion is twice higher in the shallow sample (Supplementary Table S2). Also, the microscopic analysis of JTC3 profile sections with SEM-EDS (Supplementary Table S3) detected cassiterite (Supplementary Fig. S1b), a secondary mineral of As with Fe and minor Cu (Supplementary Fig. S1e), a secondary Pb hydroxysulfate (potentially plumbojarosite) with As as a minor constituent (Supplementary Fig. S2b), and a secondary mineral of Fe oxyhydroxides with As and Al (Supplementary Fig. S2e).

The elemental concentrations of the profile samples across all the cells are presented in Table 1. Iron was the major constituent with total concentration ranging from 35 400 to 77 800 μg g^{-1}; followed by aluminum (Al) with concentrations ranging from 7220 to 21 000 μg g^{-1}. The relatively low average calcium (Ca) concentration, 356 μg g^{-1} (range 172–1030 μg g^{-1}), limits the buffering capacity in tailings and explains the low pH across the tailing profile. Among trace elements, As and Sn are the most abundant with

Table 1 Total concentration of elements in profile sections of Jumna tailing cells

Location	Sample	Depth[a] (cm)	pH[b]	ORP (mV)	Cu	Zn	Na	Ca	Mg	Fe	Al (μg g⁻¹)	K	P	Mn	As	Pb	Sn
JTC1	JTC1-1	0–40	4.4	330	420	637	157	745	2710	72 500	19 000	4230	306	803	683	335	2510
	JTC1-2	40–90	4.6	313	447	414	139	533	2260	70 500	17 600	3420	346	614	1570	509	2320
	JTC1-3	90–140	4.4	311	445	447	127	525	2380	77 800	18 900	3610	381	578	1070	674	2630
JTC2	JTC2-1	0–5	3.6	372	503	480	433	596	2730	66 900	17 400	4580	349	600	867	419	2250
	JTC2-2	5–15	4.0	350	343	195	432	227	2220	61 400	15 300	4550	362	375	889	412	2080
	JTC2-3	15–25	3.9	347	240	136	259	172	1640	45 700	11 100	3300	265	271	565	227	1640
	JTC2-4	25–35	3.9	353	361	196	443	187	2160	64 300	15 300	4790	347	352	957	435	2280
	JTC2-5	35–45	3.7	358	511	222	355	212	2340	67 600	15 800	5270	393	372	1070	481	2280
	JTC2-6	45–55	3.9	350	368	191	335	177	2090	64 900	13 600	4800	327	328	1150	510	1980
	JTC2-7	55–65	3.9	347	228	121	199	189	1570	42 300	9140	2890	207	261	592	212	1300
	JTC2-8	65–75	3.8	352	411	212	338	241	2090	66 500	14 700	4770	394	346	1010	375	2190
	JTC2-9	75–85	4.0	343	306	150	226	197	1820	51 900	11 900	4330	329	270	553	200	1810
	JTC2-10	85–180	4.0	327	1230	645	187	1030	3430	67 500	19 300	4280	409	821	498	424	2650
JTC3	JTC3-1	0–30	4.8	293	534	127	67	491	1270	56 600	9840	1640	365	367	2980	216	1560
	JTC3-2	30–130	4.7	298	333	111	62	397	1280	47 600	9540	1660	278	321	2080	206	1470
JTC4	JTC4-1	0–15	3.4	373	381	166	264	345	2080	43 600	8240	6280	95	537	1120	128	1290
	JTC4-2	15–75	3.9	347	188	96	86	263	1680	35 400	7220	3400	220	215	458	68	1070
	JTC4-3	75–125	4.5	360	1870	185	132	414	3710	57 700	21 000	7270	196	416	296	54	2910

[a]Depth is the composited interval below the surface

[b]pH was measured in a wet paste

Concentrations of the elements are in μg g⁻¹ of each in the bulk tailing samples at each depth sampled

Fig. 2 Panoramic pictures of the cells at Jumna tailings facility: **a** waste dump located at JTC1; **b** hardpan at JTC3; **c** copper sulfate (CuSO₄) efflorescence at JTC4 close to the pond; **d** tailing profile at JTC4, sulfidic tailings at the bottom

maximum concentrations of 2980 µg g^{-1} and 2910 µg g^{-1}, respectively. Minor trace elements are lead (Pb), copper (Cu), and zinc (Zn), although the bottom samples of JTC2 and JTC4 present higher concentration of Cu compared to the other samples (1230 and 1870 µg g^{-1}, respectively). Statistical analysis of all the profile tailing samples showed that Fe and Al are correlated ($p < 0.05$) with phosphorous (P), manganese (Mn), Pb, and Sn (Supplementary Table S4). In JTC2, Cu, Mn, As, Sn, and Fe are strongly correlated across the different depths (Supplementary Fig. S3a). Similarly, in the oxidized zone of JTC4, all those elements are highly correlated, but in the unoxidized zone (bottom profile), the Cu concentration is highest compared to the shallow samples, and As concentration, in contrast, is the lowest (Supplementary Fig. S3b).

The water sample collected from JTC4 dam reveals an acidic environment with pH = 2.6, and EC = 2.9 mS cm^{-1} (Supplementary Table S5). The concentrations of the elements in water follow a sequence of increasing abundance: K < Sn < Cu < Zn < Fe < Mg < Al < Mn < Ca, with high concentrations of Mn (7.83 mg L^{-1}), Cu (1.11 mg L^{-1}), and Zn (3.11 mg L^{-1}), followed by Sn (545 µg L^{-1}), Pb (9.9 µg L^{-1}), and Cd (12.3 µg L^{-1}). The concentrations of As and sodium (Na) were below the limit of detection, 8.4 µg As L^{-1}, and 303.8 µg Na L^{-1}, respectively.

3.2 Fractionation by Sequential Extraction Procedure

The SEP scheme was applied to selected samples with the highest concentrations of As (JTC3-1 and JTC3-2), and the results are shown in Table 2 and Figure 3. In sample JTC3-1, As was mostly present in the crystalline Fe oxide–bound fraction (75% of total As) and in the amorphous and poorly crystalline Fe (oxy) hydroxide–bound fraction (21% of total As). The percentage of As associated with primary sulfides (3% of total As) and secondary sulfides (0.4% of total As) was very low. Similarly, the specifically sorbed fraction of As was very low and accounted for only 0.9% of total As. Arsenic was not detected either in the water-soluble or in the exchangeable fraction, which is a relevant feature considering that both fractions are the most easily leachable exerting direct ecological toxicity. The As partitioning for sample JTC3-2 is similar to that for JTC3-1, but with slightly higher As concentration (78% of total As) in the crystalline

Fe-oxide fraction and slightly lower As concentration (17% of total As) in the amorphous and poorly crystalline Fe-(oxy)hydroxide–bound fraction. Iron in both JTC3-1 and JTC3-2 was mostly found as crystalline Fe-oxides (64% of total Fe), and as primary sulfides (25% of total Fe), followed by the amorphous and poorly crystalline Fe-(oxy)hydroxides (11% of total Fe), while the rest of the fractions altogether account less than 1% of total Fe content. Since Sn is present in the studied tailings as oxide mineral, and bearing in mind that the applied SEP was not tailored for Sn, therefore, for this element, the secondary and primary sulfide fractions of the SEP actually remain in the residual fraction, similarly to other oxides, *i.e.* wolframite (Li et al., 2019). Tin, different from As and Fe, is mostly present in both JTC3-1 and JTC3-2 in the residual fraction (52% of total Sn) followed by the crystalline Fe-oxide fraction (33% of total Sn), and the amorphous and poorly crystalline Fe-(oxy) hydroxide fraction (14% of total Sn). Regarding Cu, in JTC3-1 and JTC3-2 samples, on average, most of this metal was found as crystalline Fe-oxide fraction (55% of total Cu), and as amorphous and poorly crystalline Fe-(oxy)hydroxide fraction (38% of total Cu), followed by primary sulfide fraction (6% of total Cu). The rest of the fractions account altogether for only 1% of total Cu in the tailings. Manganese exhibits a similar partitioning to that for Sn, although the percentages in the water-soluble, exchangeable, and specifically sorbed fractions are higher than those of Sn and other elements (As, Cu, and Fe), accounting for 2%, 3%, and 4% of total Mn, respectively (Fig. 3).

3.3 Elemental Concentrations in Plants and Substrate

The identification of plants and elemental analysis of the substrate and plant samples are presented in Tables 3 and 4, respectively. This is very challenging for plants to establish (Fig. 4) given that the average pH is 4, which ranges down to pH 3.5 for the submerged plant (sample JTC4-S1) to pH 5.2 (sample JTC1-S5). Among the studied elements, Fe has the highest concentrations in the substrate with an average concentration of 46 400 µg Fe g^{-1} (range 34 700–61 100 µg Fe g^{-1}), followed by Al (9810 µg Al g^{-1} average concentration, range 7920–12,400 µg Al g^{-1}), K (2320 µg K g^{-1} on average, range 1140–6280 µg K g^{-1}), Mg (1440 µg Mg g^{-1} on average, range 654–2080 µg Mg g^{-1}), and Sn w(1500

Table 2 Fractionation of elements in Jumna tailings samples JTC3-1 and JTC3-2

Sample	Extractant	As	Cu	Ca	Mg	Mn	Fe	K	Al	Pb	Sn
							(μg g^{-1})				
JTC3-1	Water-soluble As	LOD	0.32 ± 0.13	64 ± 36	21 ± 12	11 ± 6	3 ± 3	143 ± 79	9 ± 5	LOD	4 ± 3
	Exchangeable As	LOD	0.35 ± 0.10	60 ± 8	20 ± 2	14 ± 1	6 ± 1	58 ± 8	6 ± 0.66	LOD	4 ± 2
	Specifically sorbed As	28 ± 5	1 ± 0.23	37 ± 6	21 ± 3	12 ± 2	6 ± 6	24 ± 4	12 ± 6	LOD	8 ± 1
	Amorphous and poorly crystalline Fe-(oxy) hydroxide–bound As	652 ± 175	245 ± 62	31 ± 7	28 ± 7	41 ± 11	7312 ± 1913	17 ± 8	1360 ± 373	LOD	417 ± 102
	Crystalline Fe-oxides	2380 ± 130	296 ± 11	64 ± 5	265 ± 13	122 ± 20	40 000 ± 1740	157 ± 8	2890 ± 155	113 ± 26	1010 ± 50
	Secondary sulfides	13 ± 5	3 ± 0.71	19 ± 3	24 ± 5	4 ± 2	366 ± 108	142 ± 37	723 ± 173	10 ± 3	220 ± 56
	Primary sulfides	94 ± 7	33 ± 2	230 ± 9	795 ± 31	209 ± 37	15 800 ± 680	1120 ± 40	4700 ± 171	104 ± 19	1390 ± 61
JTC3-2	Water-soluble As	LOD	0.20 ± 0.11	38 ± 24	12 ± 8	6 ± 4	2 ± 1	92 ± 53	6 ± 3	LOD	2 ± 1
	Exchangeable As	LOD	0.26 ± 0.10	58 ± 4	19 ± 0.84	12 ± 1	4 ± 0.94	53 ± 1	6 ± 2	LOD	5 ± 3
	Specifically sorbed As	30 ± 2	1 ± 0.09	40 ± 1	23 ± 0.47	15 ± 0.77	6 ± 7	25 ± 1	14 ± 7	LOD	5 ± 2
	Amorphous and poorly crystalline Fe-(oxy) hydroxide–bound As	438 ± 55	131 ± 18	29 ± 5	23 ± 3	30 ± 8	5690 ± 996	LOD	1110 ± 212	30 ± 31	384 ± 63
	Crystalline Fe-oxides	2040 ± 163	218 ± 6	60 ± 1	303 ± 8	129 ± 33	34 300 ± 1680	177 ± 9	3000 ± 76	112 ± 31	1010 ± 50
	Secondary sulfides	12 ± 4	2 ± 0.71	13 ± 0.62	16 ± 11	4 ± 2	175 ± 127	95 ± 87	471 ± 447	LOD	130 ± 134
	Primary sulfides	74 ± 14	23 ± 2	154 ± 7	767 ± 31	179 ± 17	12 300 ± 401	1080 ± 44	4500 ± 158	120 ± 34	1350 ± 28

Values are means ± relative standard deviation, where $n = 6$

LOD: Below the limit of detection, As LOD: 0.019 μg g^{-1}, K LOD: 0.033 μg g^{-1}, Pb LOD: 0.366 μg g^{-1}
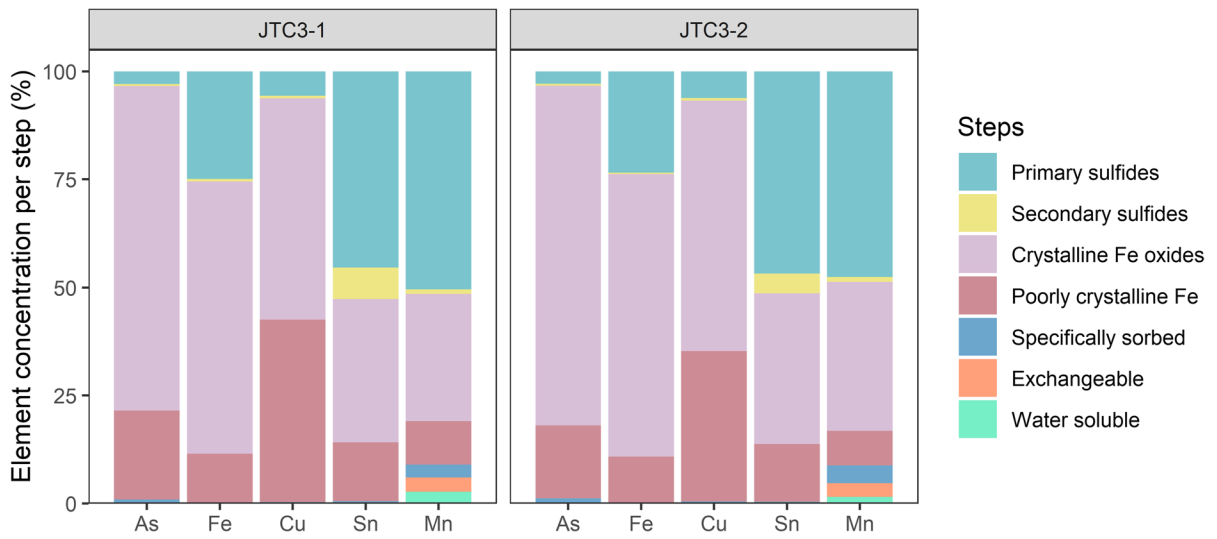
Fig. 3 Fractionation of As, Cu, Fe, Sn, and Mn (% of total concentration) by the sequential extraction procedure in samples JTC3-1 and JTC3-2

Table 3 Total concentration of elements in the soil substrate of plant samples collected at Jumna tailing cells

Location	Sample	pH	ORP (mV)	Cu	Zn	Na	Ca	Mg	Fe	Al	K	P	Mn	As	Pb	Sn
										(μg g^{-1})						
JTC1	JTC1-S1	4.7	252	115	95	60	270	2030	45 300	11 600	1140	286	364	337	304	1550
	JTC1-S2	4.4	288	205	180	125	320	1670	52 100	12 200	2650	286	499	441	266	1740
	JTC1-S3	4.5	288	179	183	84	486	1480	47 900	10 600	1860	245	340	450	319	1660
	JTC1-S4	4.1	313	169	221	140	374	1570	50 600	10 800	1700	295	375	476	509	1620
	JTC1-S5	5.2	263	190	141	74	290	1160	34 700	8020	1460	194	266	237	168	1210
	JTC1-S6	4.9	284	258	148	93	247	1660	46 300	11 200	2400	281	369	336	154	1720
	JTC1-S7	4.9	279	248	166	108	266	1320	46 800	9840	2220	315	250	427	275	1480
	JTC1-S8	4.9	275	212	135	99	192	1200	43 100	8720	2020	246	217	336	185	1440
JTC2	JTC2-S1	3.7	343	252	150	131	219	1660	41 000	8920	2880	298	265	465	163	1350
	JTC2-S2	3.7	342	265	125	115	156	1370	41 300	8630	2320	215	239	486	181	1340
	JTC2-S3	4.1	326	170	97	107	171	1250	37 200	8100	1780	211	228	378	152	1280
	JTC2-S4	4.0	338	232	140	352	312	1280	40 300	9490	2610	268	247	459	160	1400
	JTC2-S5	4.5	308	249	178	158	206	1920	52 800	12 400	3150	319	343	498	293	1810
	JTC2-S6[a]	5.1	259	491	101	114	236	654	35 400	10 700	1500	280	179	254	107	1490
JTC3	JTC3-S1	4.6	317	452	156	100	572	1290	56 300	9540	1520	373	464	2421	193	1620
JTC4	JTC4-S1	3.5	337	239	161	161	522	809	61 100	7920	1660	275	232	248	217	1360
	JTC4-S2	3.6	344	207	213	176	1220	1510	58 700	9660	2560	275	394	409	207	1570
	JTC4-S3[b]	3.4	373	381	166	264	345	2080	43 600	8240	6280	95	537	1125	128	1290

Soil samples were collected from plant roots (depth~20 cm)

pH was measured on wet paste

Concentrations of the elements are in μg g^{-1} of each in the soil sample

[a]These results are also considered for the S7 and S8 due to proximity of samples

[b]These results are considered from the surface sample of JTC4-1 tailings profile sample due to proximity of the plant

Table 4 Total concentration of elements in plant shoot samples (dry weight) collected in the Jumma tailing cells

Location	Sample	Identification	Cu	Zn	Na	Ca	Mg	Fe	Al (µg g⁻¹)	P	K	Mn	As	Pb	Sn
JTC1	JTC1-P1	*Eucalyptus* sp.	8	784	560	11 400	1210	98	255	1670	6120	4780	8	LOD	4
	JTC1-P2	*Eucalyptus* sp.	10	201	80	1780	1850	57	50	1190	14 100	763	LOD	3	LOD
	JTC1-P3	*Eucalyptus* sp.	5	338	138	1840	799	70	87	1030	5060	906	1	LOD	4
	JTC1-P4	*Acacia* sp.	13	106	1520	1880	1110	61	29	412	3890	203	5	LOD	2
	JTC1-P5	*Acacia* sp.	67	152	1080	5060	830	164	210	327	3740	133	2	3	6
	JTC1-P6	*Acacia* sp.	17	442	LOD	3790	2120	103	51	1450	11 000	1520	LOD	2	3
	JTC1-P7	*Poaceae* sp.	47	302	429	1560	576	574	298	511	2700	298	15	19	7
	JTC1-P8	*Poaceae* sp.	7	286	268	1210	490	147	47	618	3260	194	LOD	8	1
	JTC1-P8R	*Poaceae* sp.	147	261	LOD	459	384	2110	637	743	3090	199	40	27	2
JTC2	JTC2-P1	*Eucalyptus* sp.	33	251	250	1600	1740	76	175	1210	8700	827	LOD	16	6
	JTC2-P2	*Eucalyptus* sp.	15	164	340	1180	1930	101	155	886	9420	641	0.4	2	6
	JTC2-P3	*Callitris intratropica*	4	343	23	5860	1590	197	87	2070	10 500	1150	13	1	3
	JTC2-P4	*Acacia* sp.	6	15	8	1460	1310	318	107	274	4020	44	0.2	12	3
	JTC2-P5	*Callitris intratropica*	4	267	759	3300	1050	189	100	474	5780	1400	2	4	6
	JTC2-P6	*Jacksonia* sp.	1	22	773	2340	567	35	LOD	192	5490	272	LOD	15	4
	JTC2-P7	*Acacia* sp.	5	20	694	2270	785	68	32	258	8310	124	3	5	3
	JTC2-P8	*Acacia* sp.	2	14	352	4180	944	35	23	165	2740	74	12	15	3
JTC3	JTC3-P1	*Poaceae* sp.	39	89	240	3410	2490	606	246	878	19 300	1250	21	7	8
JTC4	JTC4-P1	*Eleocharis equisetina*	73	216	2550	1030	1440	246	297	742	25 300	480	LOD	4	6
	JTC4-P1R	*Eleocharis equisetina*	325	443	1450	440	559	2420	1200	681	11 400	335	12	14	LOD
	JTC4-P2	*Cyperaceae* sp.	16	423	1330	2500	3580	152	312	651	21 100	2020	4	20	6
	JTC4-P2R	*Cyperaceae* sp.	191	587	928	1570	1750	3440	2210	322	4690	904	25	46	9
	JTC4-P3	*Eucalyptus* sp.	27	96	LOD	4840	1080	35	37	1590	13 300	1050	LOD	8	6

R root analysis

Concentrations of the elements are in µg g⁻¹ of each in the living biomass of the sample in dry weight (DW)

LOD limit of detection, As LOD: 0.13 µg g⁻¹, Sn LOD: 0.08 µg g⁻¹

Fig. 4 Plants advantageously colonising the tailings and bund walls: **a** *Poaceae* sp. in JTC1; **b** *Callitris intratropica* in JTC2; **c** *Acacia* sp. in JTC2; **d** *Poaceae* sp. in JTC3; **e** *Cyperaceae* sp. in JTC4; **f** *Eleocharis equisetina* in the pond at JTC4

µg Sn g^{-1} on average, range 1210–1810 µg Sn g^{-1}) (Table 3). Other elements such as Ca, Cu, Zn, Pb, and P are also present at concentrations of around 300 µg g^{-1} each (Table 3). The average concentration of As is 433 µg g^{-1} across JTC1, JTC2, and JTC4, and only at JTC3-S1 (*Poaceae* sp.) the substrate has extremely high concentrations of As (2420 µg As g^{-1}), while the lowest As concentration is 237 µg As g^{-1} in sample JTC1-S5 (Table 3).

For all of the plants, the average concentration of the major elements in the shoots follows the decreasing sequence: K (9200 µg g^{-1}) > Ca (3120 µg g^{-1}) > Mg (1380 µg g^{-1}). Lower concentrations of Mn > P > Na > Zn > Fe > Al were present with the following averages: 906 µg Mn g^{-1}, 831 µg P g^{-1}, 633 µg Na g^{-1}, 226 µg Zn g^{-1}, 167 µg Fe g^{-1}, and 137 µg Al g^{-1}. Regarding the trace metal(loid)s, Cu concentrations in the shoots were 20 µg g^{-1} on average, but higher concentrations (up to 20-fold) of this metal were found in the roots of the analysed plant samples (221 µg Cu g^{-1} on average) (Table 4). For example, *Poaceae* sp. contains 7 µg Cu g^{-1} in their shoots and 147 µg Cu g^{-1} in the roots, *Eleocharis equisetina* has 73 µg Cu g^{-1} in their shoots and 325 µg Cu g^{-1} in the roots, and *Cyperaceae* sp. has 16 µg Cu g^{-1} in their shoots and 191 µg Cu g^{-1} in their roots (Table 4). Very low concentrations of Pb and Sn were found in

the shoots (< 10 µg g^{-1} on average). Similarly, low concentrations of As were found in the shoots (7 µg As g^{-1} on average), and in some samples it was below the limit of detection. Analysis of the roots revealed higher concentrations of As compared to the shoots. For example, *Poaceae* sp. contains < 0.13 µg As g^{-1} in their shoots and 40 µg As g^{-1} in the roots, *Eleocharis equisetina* has a concentration of As < 0.13 µg As g^{-1} in its shoots and of 12 µg g^{-1} in the roots, while *Cyperaceae* sp. has 4 µg As g^{-1} in its shoots and 25 µg g^{-1} in the roots (Table 4 and Fig. 5).

3.4 Metal(loid) Enrichment Factor

The results of the ER comparing the element concentration of tailing samples with the Australian background concentrations are presented in Supplementary Table S6. According to the ER, the Jumna tailings can be categorized as extremely enriched with As and Sn, for which most of the samples (94% and 100%, respectively) present ER > 40 (ER_{As} = 93 and ER_{Sn} = 436). In the case of Cu, 39% of the studied samples show extreme presence (ER > 40) and the 61% very strong excess (ER between 20 and 40). The ER for Pb yielded significant presence, since 89% of the samples have an ER between 5 and 20. Regarding Zn, 72% of the samples equally present

Fig. 5 Bars showing the As concentrations ($\mu g\ g^{-1}$) in shoots and substrate of plant species growing at the Jumna tailings facility
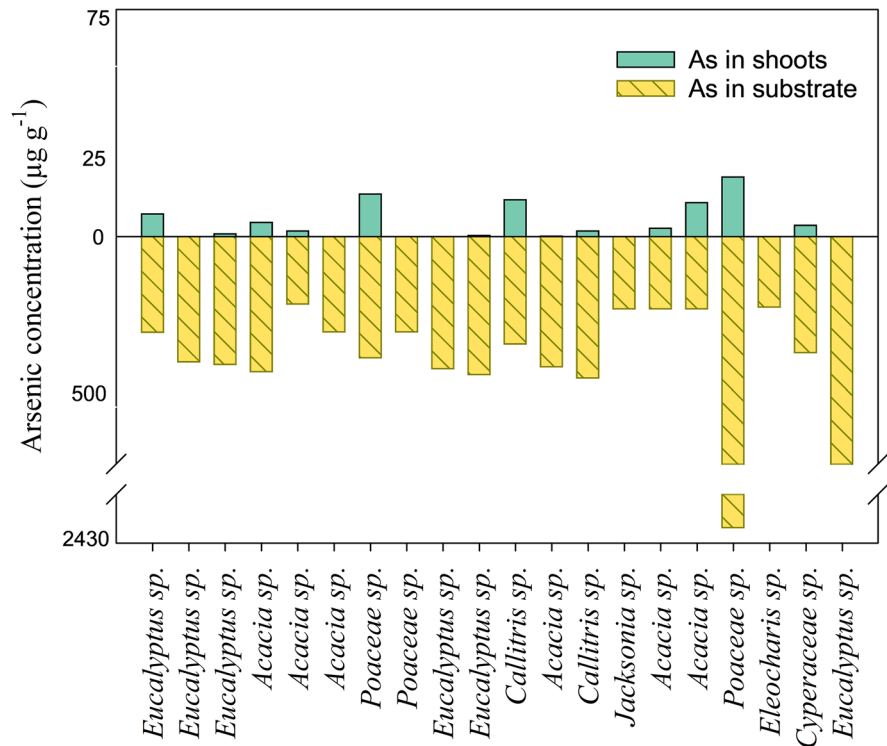
ER < 2 (minimal pollution category), while the other 28% of the samples yielded ER between 5 and 20, indicating moderate presence of this metal. Most of the samples are classified as minimally polluted for Na and Mn with 89% and 78% of the samples, having ER < 2, respectively. In the case of K, 72% of the samples represent moderate pollution (ER between 2 and 5), and 22% minimal pollution (ER < 2). Other elements such as Ca, Mg, Fe, and Al are categorized in the minimal pollution category based on 100% of the samples with ER < 2.

4 Discussion

As the Jumna tailings were left uncapped and exposed to the environment in the late 1980s, oxidation processes resulted in the formation of AMD and, subsequently, of secondary minerals (*e.g.* Fe-oxyhydroxides loaded with As). Currently, the cells JTC1, JTC2, and JTC3 have well-oxidized profiles and a hardpan has formed at the surface. In contrast, cell JTC4 has an unoxidized bottom layer that has fresh sulfidic tailings with very high Cu concentrations (1870 $\mu g\ g^{-1}$), and also shows evident efflorescences

its surface (Fig. 2c). This may be explained by the diversity of the cassiterite-rich ore deposits processed at Jumna, *e.g.* the Baal Gammon mine mainly has Cu sulfides, but this porphyry deposit was also rich in cassiterite (Garrad & Bultitude, 1999). The reason for the occurrence of this unoxidized layer is that JTC4 has a permanent pond, which prevents oxygen to enter into the tailings (Brett, 2009).

Across the Jumna tailing profiles, the pH is in the mildly acidic range and on average has a value of pH ~4, hence the potential of AMD formation is in the medium range (Yucel & Baba, 2016). This can be explained by the low buffering capacity of the tailings given that calcite is only present as a trace mineral in the JTC2 and JTC3 cells, and dolomite was not detected by the XRD analysis. Even though chlorite was detected the Ca content is on average only < 400 $\mu g\ g^{-1}$ and that of Mg is ~2000 $\mu g\ g^{-1}$, compared to ~59 000 $\mu g\ g^{-1}$ of Fe. In general, in the initial stages of AMD formation, calcite and dolomite are easily weathered (Jambor, 2003), although silicate minerals such as chlorite, hornblende, and albite can provide some buffering capacity (Peikam & Jalali, 2017). Arsenopyrite was not identified in the SEM-EDS analysis, instead secondary minerals of As were observed

(Supplementary Fig. S1e and S2e). In addition, the sequential extraction procedure showed that only ~2% of the As is associated to the primary sulfide fraction (Table 2 and Fig. 3). In mine wastes where arsenopyrite is present, due to the highest oxidizing rate in low pH media, this mineral becomes more reactive with a dissolution five times faster that of pyrite (McKibben et al., 2008; Rimstidt et al., 1994). It is important to note that pyrite and pyrrhotite are the main precursors of AMD (Jambor, 2003) and also the most abundant sulfide minerals in tailings (Vaughan & Corkhill, 2017). In polymetallic ore deposits, the AMD leads to the dissolution of other sulfides as well (*e.g.* sphalerite and galena) releasing associated toxic pollutants (Vaughan, 2006). Following this process at Jumna, a secondary Pb hydroxysulfate (possibly plumbojarosite) with intact relics was also observed with SEM-EDS (Supplementary Fig. S2b, S2c).

As shown by SEP partitioning, the majority of the As in Jumna tailings is in the crystalline Fe-oxide fraction (between 75% in JTC3-1 and 78% of total As in JTC3-2); in agreement, the XRD analysis reports goethite contents of 3.7% and 2.7% in JTC3-1 and JTC3-2, respectively. Goethite exhibits affinity for As and has a high capacity to sorb As, albeit lower than that of amorphous Fe-oxides (Asta et al., 2009; Craw & Bowell, 2014; Paktunc, 2013). The second highest SEP fraction is the amorphous and poorly crystalline Fe-(oxy) hydroxide one (21% in JTC3-1 and 17% of total As in JTC3-2), accounting both fractions together for 95% of As in both profile samples (Fig. 3). Once As is released from the oxidized arsenopyrite, it is naturally attenuated by Fe precipitates, thereby limiting As mobility (Craw & Bowell, 2014). It is important to note that the release of As from arsenopyrite is even faster than the dissolution of the mineral itself (McKibben et al., 2008). Arsenite (As^{III}) and arsenate (As^V) exhibit a strong affinity to Fe hydroxides and oxyhydroxides, such as ferrihydrite and goethite, and to Al oxyhydroxides and Mn oxides when Fe concentrations are lower (O'Day, 2006). Arsenic can also be adsorbed or co-precipitated as a trace element in goethite ($FeOOH$) and jarosite ($KFe_3(SO_4)_2(OH)_6$) as well as in poorly crystalline and amorphous Fe-Al precipitates (Courtin-Nomade et al., 2005, 2009).

Similar to the results of the As partitioning, the bulk of As was found associated to the oxide fraction in sediments affected by mine waste, *e.g.* 57% of As in the sediments of Moira Lake, Ontario, Canada (Azcue & Nriagu, 1995), and 53% of As in

the sediments of AMD of the mine Mount Bischoff, Tasmania, Australia (Gault et al., 2005). In the latter, the amorphous/poorly crystalline plus the Fe and Al oxides account together for ~92% of total As (Gault et al., 2005). In mine tailings, the most common As-bearing secondary mineral is scorodite, followed by Fe^{III} oxyhydroxides, and ferric arsenates. However, as the As-hosting minerals are heterogeneous, they are difficult to detect by routine methods (Paktunc et al., 2008). However, automated mineral liberation analysis (MLA) (Redwan & Rammlmair, 2012) and synchrotron-based methods are able to identify these minerals. For example, X-ray absorption near-edge spectroscopy (XANES) analysis of mine wastes in Australia has shown that the majority of As is located within iron arsenate minerals (Diacomanolis et al., 2016; Matanitobua et al., 2007).

At the Jumna tailings, As can be potentially released from the amorphous/and poorly crystalline fraction, which accounts for the 19% of the total As (~550 µg As g^{-1}). Indeed, it has been widely reported that the fate of As relies on the behaviour of elements, such as Fe (Paktunc et al., 2008). The highly common, poorly crystalline Fe^{III} oxides (ferrihydrites) are thermodynamically unstable, and with time transform to more crystalline Fe^{III} oxides such as goethite and hematite (Kukkadapu et al., 2003). However, goethite and hematite have lower sorption availability for As^V than ferrihydrite, and as a result arsenate is released (Paktunc et al., 2008). The As release from secondary minerals is also controlled by the pH, for example, the solubility of scorodite is high for both extremely acid pH and in neutral to alkaline pH (Blowes et al., 2014; Majzlan et al., 2012; Paktunc et al., 2008). Besides, biotic reduction of As^V to As^{III} due to bacteria activity can release arsenic as As^{III} species (Burnol et al., 2007), which are generally more mobile and toxic (Sharma & Sohn, 2009). The reduction of Fe^{III} oxyhydroxide with adsorbed As induce the release of this As, and this reaction can be also driven by microorganisms (O'Day et al., 2004).

Tin is mostly bound to non-mobile fractions in Jumna tailings (primarily in the residual fraction). In agreement with our results, Sn was mainly comprised in the residual fraction in tailings from a former cassiterite mine in Portugal (Favas et al., 2011). Furthermore, in the literature, it is reported that Sn bioavailability is low (Rüdel, 2003). Cassiterite is one of the main minerals of Sn (Cima, 2011), and

due to its low solubility constant ($Ksp = 10^{-64.2}$) (Rai et al., 2011), this mineral is stable under acidic conditions (Romero et al., 2014). As cassiterite is a refractory compound, it dissolves at high temperatures (> 700 °C) (Navrotsky, 2014), and remains insoluble at room temperature in aqueous media (Haase et al., 2021). The release of Sn to the environment depends on the precipitation of Sn hydroxides (schoenfliesite group), which can be formed (i) as primary minerals in hydrothermal systems; (ii) weathering of Sn sulfide minerals; and potentially cassiterite (Haase et al., 2021). At Jumna, Sn predominantly exists as cassiterite as reported in the XRD and SEM analysis, a stable and poorly soluble mineral form, which explains that the major proportion in tailings was found in the residual fraction of the SEP, and thus is poorly mobile and bioavailable.

Plants typically grow in soils with only 0.1–10 µg g^{-1} As background concentrations (Mirza et al., 2014; Reeves et al., 2018); however, noteworthy all plant species collected at Jumna tolerate much higher concentrations with up to 400 µg As g^{-1}. This may be explained because metal(loid)s bound to Fe-phases are not available for plants, while usually the sum of water-soluble, exchangeable and carbonate fractions are considered to be most easily leachable and bioavailable (Azcue & Nriagu, 1995; Sidenko et al., 2007). In the current study, SEP showed the water-soluble and exchangeable As were both negligible, and we considered the specifically sorbed As as the bioavailable As fraction (~30 µg As g^{-1}) (Table 2). Even though the specifically sorbed fraction of As is strongly retained, As could be mobilised by ligand exchange with phosphate or other anions, thus becoming bioavailable, or partially taken up by plants, and therefore this As fraction is assumed as potentially bioavailable (Smith et al., 2008; Tang et al., 2007). The results showed that among the plants, *Eleocharis equisetina, Cyperaceae* sp., and *Poaceae* sp. have a [leaf]/[root] ratio of As concentration <1 (Table 4); hence, these species can be categorized as 'excluders' because they do not translocate from the soil metal(loid)s to the shoots (Baker, 1981, 1987). These findings correlate with the typical observed behaviour for As at a global scale where the As accumulated in the plants (1.8×10^5 t As) (Markert, 1992) is lower compared to the As in the soil (1.7–2.5×10^9 t As) (Wenzel, 2013), and this accumulation is higher in roots compared to the shoots

(Zhao et al., 2009), seeds, or fruits (Matschullat, 2011). This can be explained because As bioaccumulation is limited due to the general low bioavailability of As in the soil (Bowell et al., 2014). Furthermore, the analysed plants at Jumna accumulate <10 µg Sn g^{-1} (Table 4), even though the Sn concentration in the soil is on average 1500 µg Sn g^{-1} (Table 3), which is in agreement with the low bioavailable Sn in the SEP results (Table 2, Fig. 3). The rate of Sn translocation to plants is typically 100 times lower compared to Sn concentration in the soil, and some crops accumulate up to 9 µg Sn g^{-1} (Cima, 2011).

Characterization of the Jumna tailings indicate predominance of some metal(loid)s accordingly with its precedence from an orebody, the enrichment ratio attributed As and Sn as the major elements and contributor for the overall contamination of the Jumna tailings. Albeit the ER frames a general scale of contamination without considering geochemical processes, the outcome provides prioritization of toxic elements for further assessment and remediation (Kowalska et al., 2018). According to the Australian National Protection Measure (NEPM), the Ecological Investigation Levels (EILs) for aged As (contamination for over 2 years) ranges from 40 µg g^{-1} for areas of ecological significance to 160 µg g^{-1} for commercial and industrial soil (National Environmental Protection, 2013). The As concentrations at Jumna tailings exceeded the NEPM ecological levels set for As (Table 1). Also, the water samples from the pond at cell JTC4 contain high concentrations of Cu, Zn, Cd, Sn, and Pb (Supplementary Table S5). Comparing these concentrations with water quality values set for aquatic ecosystems according to the Australian and New Zealand Water Quality Guidelines (2018), they are higher than the threshold considered for the 80% level of protection of species, which establish the following limits: 2.5 µg Cu L^{-1}, 31 µg Zn L^{-1}, 0.8 µg Cd L^{-1}, and 9.4 µg Pb L^{-1}. In the case of As, the concentrations recorded in this study were below the limit of detection (8.4 µg As L^{-1}), and did not exceed the guidelines for 80% level of species protection, which establish 360 µg L^{-1} for As^{III} and 140 µg L^{-1} for As^{V} (ANZECC and ARMCANZ, 2018).

In conjunction with the results of the partitioning of As through SEP, a general concept of the fate of As and Sn in the system can be drawn. The As fractions that are potentially available for biota represent less than 1% (~30 µg As g^{-1}) of total As in the studied

tailings (Table 2). Tin is even less bounded to bio-available fractions 0.5% (~2 μg As g^{-1}), and mostly associated to stable fractions. The fraction that could potentially release significant amounts of As is the amorphous/and poorly crystalline fraction, which accounts for around 19% (~550 μg As g^{-1}) of total As in the tailings, if eventually Fe crystallizes into goethite or hematite (Paktunc et al., 2008) or upon significant changes in the physico-chemical (Eh-pH) conditions. Even though the major fraction of As is in the crystalline Fe oxide fraction, which attenuates As, further research is required to address the stability and potential release of As from these crystalline Fe oxides upon changes in environmental conditions. In the case of Sn, especially in the oxide form, it requires further studies to tailor a SEP for tailings, and to understand the fate of this metal in relation to other major elements in the tailings.

5 Conclusions

This research investigated the geochemistry, mobilisation, and bioavailability of As, Sn, and other metals in tailings and plant species at Jumna facility, a former reprocessing plant of tailings coming from multisource cassiterite deposits. The study showed that currently the tailing cells are well oxidized and present major concentrations of As and Sn. The pH is low across the tailings and the buffering capacity is limited due to the lack of carbonate minerals. The pond water located in JTC4 contains high concentrations of Cu, Zn, Cd, and Pb. Even though the total As concentrations in the tailings are high, the dissolved As concentrations in water were below the limits of detection, which supports the restricted leaching of As in the studied tailings. The negligible concentrations of water-soluble and exchangeable As suggest that immediate mobilisation of As from the tailings is unlikely. Similarly, the specifically sorbed fraction, which could be desorbed (at least partially) by ligand exchange, accounts for slightly higher 1% of the total As. Conversely, the percentage of As that could be potentially released from the amorphous and poorly crystalline Fe oxides due to their crystallization accounts for the 19% of the total As in tailings. Also, although major fraction of As was found in the crystalline Fe oxide–bound *operational* fraction, which is generally considered poorly mobile and therefore not

bioavailable, further research is required to confirm this aspect. These results are beneficial for the rehabilitation of the site, and call for attention to develop strategies to contain As, as the fate of this toxic element is not only subjected to the geochemistry of the site, but also the climatic conditions. For example, changing moisture and redox conditions inside tailings may destabilize cemented layers and release As through desorption.

Plants collected at thesite have shown the capacity to tolerate unfavourable As, Sn, and other metal(loid)-rich conditions. These plants all behave as excluders accumulating metal(loid)s in their roots and limiting the translocation to the above-ground tissues. Therefore, these plants are suitable to be used for further remediation (*i.e.* phytostabilization) of the Jumna tailings and other mine sites, although further studies are required to address the complex changes in the geochemistry of the tailings when plants thrive there.

Finally, comprehensive characterization of mine tailings is fundamental for informing rehabilitation strategies. This interdisciplinary research on abandoned tailings enriched with As presents a range of methods that can be used to develop actions to prioritize the remediation of these legacies in Australia and worldwide. The identification of native plants growing in abandoned tailings and the quantification of metal(loid) bioavailability and accumulation are key factors for the screening and discovery of metallophytes that can potentially be used for phytostabilization and phytoextraction of past and current mining projects.

References

ANZECC & ARMCANZ (2018). National water quality management strategy, Australian and New Zealand guidelines for fresh and marine water quality. The Guidelines, in A. a. N. Z. E. a. C. C. a. A. a. R. M. C. o. A. a. N. Zealand (Ed.)Canberra, Australia, Australian and New Zealand Environment and Conservation Council and Agriculture and Resource Management Council of Australia and New Zealand.

Ashley, P. M., & Lottermoser, B. G. (1999). Arsenic contamination at the Mole River mine, northern New South Wales. *Australian Journal of Earth Sciences, 46*, 861–874.

Asta, M. P., Cama, J., Martínez, M., & Giménez, J. (2009). Arsenic removal by goethite and jarosite in acidic conditions and its environmental implications. *Journal of Hazardous Materials, 171*, 965–972.

Azcue, J. M., & Nriagu, J. O. (1995). Impact of abandoned mine tailings on the arsenic concentrations in Moira Lake. *Ontario, Journal of Geochemical Exploration, 52*, 81–89.

Baker, A. J. M. (1981). Accumulators and excluders: Strategies in the response of plants to heavy metals. *Journal of Plant Nutrition, 3*, 643–654.

Baker, A. J. M. (1987). Metal tolerance. *New Phytologist, 106*, 93–111.

Blowes, D. W., Jambor, J. L., Hanton-Fong, C. J., Lortie, L., & Gould, W. D. (1998). Geochemical, mineralogical and microbiological characterization of a sulphide-bearing carbonate-rich gold-mine tailings impoundment. *Joutel, Québec, Applied Geochemistry, 13*, 687–705.

Blowes, D. W., Ptacek, C. J., Jambor, J. L., Weisener, C. G., Paktunc, D., Gould, W. D., & Johnson, D. B. (2014). *The geochemistry of acid mine drainage*. In H. D. Holland & K. K. Turekian (Eds.), *Treatise on geochemistry Oxford* (pp. 131–190). Elsevier.

Bowell, R. J., Alpers, C. N., Jamieson, H. E., Nordstrom, D. K., & Majzlan, J. (2014). The environmental geochemistry of arsenic – an overview. *Reviews in Mineralogy and Geochemistry, 79*, 1–16.

Brandstetter, A., Lombi, E., Wenzel, W. W., & Adriano, D. C. (2000). *Arsenic-contaminated soils: I. Risk assessment*. In D. L. Wise, D. J. Trantolo, E. J. Cichon, H. I. Inyang, & U. Stottmeister (Eds.), *Remediation engineering of contaminated soils* (pp. 715–737). Boca Raton CRC Press.

Brett, D. M. (2009). Water covers for tailings and waste rock — designing for perpetuity. In A. B. Fourie & M. Tibbett (Eds.), *Proceedings of the Fourth International Conference on Mine Closure* (pp. 485–492). Australian Centre for Geomechanics.

Brock, J. (1993). *Native plants of Northern Australia* (p. 355). Reed Books.

Bureau of Meterorology (2020) Climate statistics for Australian locations, Herberton. Period 1991-2020, Bureau of Meterorology.

Burnol, A., Garrido, F., Baranger, P., Joulian, C., Dictor, M.-C., Bodénan, F., Morin, G., & Charlet, L. (2007). Decoupling of arsenic and iron release from ferrihydrite suspension under reducing conditions: A biogeochemical model. *Geochemical Transactions, 8*, 12–12.

Candeias, C., Ávila, P., Coelho, P., & Teixeira, J. P. (2019). *Mining activities: Health impacts*. In J. Nriagu (Ed.), *Encyclopedia of Environmental Health* (Second ed., pp. 415–435). Elsevier.

Chaney, R. L., & Baklanov, I. A. (2017). *Phytoremediation and phytomining: Status and promise*. In A. Cuypers & J. Vangronsveld (Eds.), *Advances in Botanical Research* (pp. 189–221). Academic Press.

Cima, F. (2011). *Tin: environmental pollution and health effects*. In J. O. Nriagu (Ed.), *Encyclopedia of environmental health* (pp. 351–359). Elsevier.

Coelho, P. C. S., Teixeira, J. P. F., & Gonçalves, O. N. B. S. M. (2011). *Mining activities: Health impacts*. In J. O. Nriagu (Ed.), *Encyclopedia of Environmental Health* (pp. 788–802). Elsevier.

Cooper, M., de Caritat, P., Burton, G., Fidler, R., Green, G., House, E., Strickland, C., Tang, J. & Wygralak, A. (2010). *National geochemical survey of Australia: Field data. Geoscience Australia, Record 2010/18*, 93 pp.

Courtin-Nomade, A., Grosbois, C., Bril, H., & Roussel, C. (2005). Spatial variability of arsenic in some iron-rich deposits generated by acid mine drainage. *Applied Geochemistry, 20*, 383–396.

Courtin-Nomade, A., Grosbois, C., Marcus, M. A., Fakra, S. C., Beny, J. M., & Foster, A. L. (2009). The weathering of a sulfide orebody: speciation and fate of some potential contaminants. *Canadian Mineralogist, 47*, 493–508.

Craw, D., & Bowell, R. J. (2014). The characterization of arsenic in mine waste. *Reviews in Mineralogy and Geochemistry, 79*, 473–505.

Dash, P. H., Barker, R. M., Morwood, D. A., Culpeper, L. G. & Lam, J. S. F. (1991). Mineral occurrences - Atherton 1:100 000 sheet area. Geological Survey of Queensland Record 1991/14 Brisbane.

de Caritat, P., & Cooper, M. (2011). National geochemical survey of Australia: The geochemical atlas of Australia. *Canberra, Australia, Geoscience Australia, Record, 2011*(20), 557.

Diacomanolis, V., Noller, B. N., Taga, R., Harris, H. H., Aitken, J. B., & Ng, J. C. (2016). Relationship of arsenic speciation and bioavailability in mine wastes for human health risk assessment. *Environmental Chemistry, 13*, 641–655.

Dold, B. (2003). Speciation of the most soluble phases in a sequential extraction procedure adapted for geochemical studies of copper sulfide mine waste. *Journal of Geochemical Exploration, 80*, 55–68.

Dold, B. (2014). Evolution of acid mine drainage formation in sulphidic mine tailings. *Minerals, 4*, 621–641.

Doronila, A. I., Maddox, L. E., Reichman, S. M., King, D. J., Kolev, S. D., & Woodrow, I. E. (2014). Vegetation response of Australian native grass species redgrass (*Bothriochloa macra* (Steudel) S.T. Blake) and spider grass (*Enteropogon acicularis* (Lindl.) Lazarides) in saline and arsenic contaminated gold mine tailings: A glasshouse study. *Minerals Engineering, 56*, 61–69.

Edraki, M., Baumgartl, T., Manlapig, E., Bradshaw, D., Franks, D. M., & Moran, C. J. (2014). Designing mine tailings for better environmental, social and economic outcomes: A review of alternative approaches. *Journal of Cleaner Production, 84*, 411–420.

Favas, P. J. C., Pratas, J., Gomes, M. E. P., & Cala, V. (2011). Selective chemical extraction of heavy metals in tailings and soils contaminated by mining activity: Environmental implications. *Journal of Geochemical Exploration, 111*, 160–171.

Folguera, L., Magallanes, J., & Cicerone, D. (2016). Analysis of the environmental liabilities generated by past activities in uranium mining exploitation in the Province of Córdoba, Argentina. *Environmental Earth Sciences, 75*, 407.

Garrad, P. D., & Bultitude, R. J. (1999). *Geology, mining history and mineralisation of the Hodgkinson and Kennedy Provinces, Cairns Region, North Queensland*. Department of Mines and Energy.

Gault, A. G., Cooke, D. R., Townsend, A. T., Charnock, J. M., & Polya, D. A. (2005). Mechanisms of arsenic attenuation in acid mine drainage from Mount Bischoff, western Tasmania. *Science of the Total Environment, 345*, 219–228.

Haase, P., Christensen, H. G., Nielsen, U. G., Koch, C. B., Galazka, Z., & Majzlan, J. (2021). Stability and solubility of members of tin perovskites in the schoenfliesite subgroup, $\square_2(BSn^{4+})(OH)_6$ (B = Ca, Fe^{3+}, Mg, Mn^{2+}, Zn, Cu). *Chemical Thermodynamics and Thermal Analysis, 1-2*, 100005.

Hall, G. E. M., Vaive, J. E., Beer, R., & Hoashi, M. (1996). Selective leaches revisited, with emphasis on the amorphous Fe oxyhydroxide phase extraction. *Journal of Geochemical Exploration, 56*, 59–78.

Hass, A., & Fine, P. (2010). Sequential selective extraction procedures for the study of heavy metals in soils, sediments, and waste materials—a critical review. *Critical Reviews in Environmental Science and Technology, 40*, 365–399.

Hebbard, E. R., Wilson, S. A., Jowitt, S. M., Tait, A. W., Turvey, C. C., & Wilson, H. L. (2017). Regrowth of arsenate–sulfate efflorescences on processing plant walls at the Ottery arsenic–tin mine, New South Wales, Australia: Implications for arsenic mobility and remediation of mineral processing sites. *Applied Geochemistry, 79*, 91–106.

Jambor, J. L. (2003). *Environmental aspects of mine wastes*. In J. L. Jambor, D. W. Blowes, & A. I. M. Ritchie (Eds.), *Short Course Handbook* (Vol. 31, p. 430). Mineralogical Association of Canada.

Keon, N. E., Swartz, C. H., Brabander, D. J., Harvey, C., & Hemond, H. F. (2001). Validation of an arsenic sequential extraction method for evaluating mobility in sediments. *Environmental Science and Technology, 35*, 2778–2784.

Kowalska, J. B., Mazurek, R., Gąsiorek, M., & Zaleski, T. (2018). Pollution indices as useful tools for the comprehensive evaluation of the degree of soil contamination–a review. *Environmental Geochemistry and Health, 40*, 2395–2420.

Kukkadapu, R. K., Zachara, J. M., Fredrickson, J. K., Smith, S. C., Dohnalkova, A. C., & Russell, C. K. (2003). Transformation of 2-line ferrihydrite to 6-line ferrihydrite under oxic and anoxic conditions. *American Mineralogist, 88*, 1903–1914.

Li, R., Wang, W., Wang, S., Lin, C., Wang, X., Meng, L., & Yuan, X. (2019). Comparison of two sequential extraction procedures for tungsten fractionation in the tungsten mining soils. *RSC Advances, 9*, 35456–35462.

Lombi, E., Sletten, R. S., & Wenzel, W. W. (2000). Sequentially extracted arsenic from different size fractions of contaminated soils. *Water, Air, and Soil Pollution, 124*, 319–332.

Lottermoser, B. G. (2010a). Introduction to mine wastes. In *Mine wastes: Characterization, treatment and environmental impacts* (pp. 1–41). Springer.

Lottermoser, B. G. (2010b). *Sulfidic mine wastes, Mine wastes: Characterization, treatment and environmental impacts* (pp. 43–117). Springer.

Lottermoser, B. G., & Ashley, P. M. (2006). Mobility and retention of trace elements in hardpan-cemented cassiterite tailings, north Queensland, Australia. *Environmental Geology, 50*, 835–846.

Lottermoser, B. G., & Ashley, P. M. (2011). Trace element uptake by *Eleocharis equisetina* (spike rush) in an abandoned acid mine tailings pond, northeastern Australia: Implications for land and water reclamation in tropical regions. *Environmental Pollution, 159*, 3028–3035.

Macdonald, S. J., Jordan, G. J., Bailey, T. G., & Davidson, N. (2017). Early seedling establishment on aged Tasmanian tin mine tailings constrained by nutrient deficiency and soil structure, not toxicity. *Soil Research, 55*, 692–703.

Majzlan, J., Drahota, P., Filippi, M., Grevel, K.-D., Kahl, W.-A., Plášil, J., Boerio-Goates, J., & Woodfield, B. F. (2012). Thermodynamic properties of scorodite and parascorodite ($FeAsO_4 \cdot 2H_2O$), kaňkite ($FeAsO_4 \cdot 3.5H_2O$), and $FeAsO_4$. *Hydrometallurgy, 117-118*, 47–56.

Markert, B. (1992). Presence and significance of naturally occurring chemical elements of the periodic system in the plant organism and consequences for future investigations on inorganic environmental chemistry in ecosystems. *Vegetatio, 103*, 1–30.

Matanitobua, V. P., Noller, B. N., Chiswell, B., Ng, J. C., Bruce, S. L., Huang, D., Riley, M. & Harris, H. H. (2007). Using synchrotron-based X-ray absorption spectrometry to identify the arsenic chemical forms in mine

waste materials', in J.-Y. Choi & S. Rah (Eds.), AIP Conference Proceedings, pp. 1845-1848.

Matschullat, J. (2011). *The global arsenic cycle revisited*. In E. Deschamps & J. Matschullat (Eds.), *Arsenic: Natural and anthropogenic, Baton Rouge, United States*. Taylor & Francis Group.

McKibben, M. A., Tallant, B. A., & del Angel, J. K. (2008). Kinetics of inorganic arsenopyrite oxidation in acidic aqueous solutions. *Applied Geochemistry, 23*, 121–135.

Milson, J. (2000). *Trees and shrubs of north-west Queensland*. Dept. of Primary Industries.

Minerals Council of Australia (2017). Submission to Senate Environment and communications reference committee inquiry into the rehabilitation of mining and resources projects as it relates to Commonwealth responsibilities, Minerals Council of Australia.

Mirza, N., Mahmood, Q., Maroof Shah, M., Pervez, A., & Sultan, S. (2014). Plants as useful vectors to reduce environmental toxic arsenic content. *The Scientific World Journal, 2014*, 921581.

Murciego, A., Álvarez-Ayuso, E., Pellitero, E., Rodríguez, M. A., García-Sánchez, A., Tamayo, A., Rubio, J., Rubio, F., & Rubin, J. (2011). Study of arsenopyrite weathering products in mine wastes from abandoned tungsten and tin exploitations. *Journal of Hazardous Materials, 186*, 590–601.

National Environmental Protection (2013). Schedule B1. Guidelines on investigation levels for soils and groundwater, in O. o. P. Counsel (Ed.)Canberra.

Navrotsky, A. (2014). Progress and new directions in calorimetry: a 2014 perspective. *Journal of the American Ceramic Society, 97*, 3349–3359.

Noble, T. L., Lottermoser, B. G., & Townsend, A. T. (2016). Mobility of arsenic and environmentally significant elements in mine tailings following liming. *Australian Journal of Earth Sciences, 63*, 781–793.

Noller, B. N., Diacomanolis, V., Matanitobua, V. P., Ng, J. C. & Harris, H. H.: 2012, 'Arsenic from mining old and new: legacies and challenges', in B. N. Noller, R. Naidu, J. Bundschuh & P. Bhattacharya (Eds.), Understanding the geological and medical interface of arsenic - As 2012. Proceedings of the 4th International Congress on Arsenic in the Environment, CRC Press-Taylor & Francis Group.

Nordstrom, D. K., Blowes, D. W., & Ptacek, C. J. (2015). Hydrogeochemistry and microbiology of mine drainage: An update. *Applied Geochemistry, 57*, 3–16.

O'Day, P. A. (2006). Chemistry and mineralogy of arsenic. *Elements, 2*, 77–83.

O'Day, P. A., Vlassopoulos, D., Root, R., & Rivera, N. (2004). The influence of sulfur and iron on dissolved arsenic concentrations in the shallow subsurface under changing redox conditions. *Proceedings of the National Academy of Sciences of the United States of America, 101*, 13703–13708.

Olías, M., Cánovas, C. R., Nieto, J. M., & Sarmiento, A. M. (2006). Evaluation of the dissolved contaminant load transported by the Tinto and Odiel rivers (South West Spain). *Applied Geochemistry, 21*, 1733–1749.

Paktunc, D. (2013). Mobilization of arsenic from mine tailings through reductive dissolution of goethite influenced by organic cover. *Applied Geochemistry, 36*, 49–56.

Paktunc, D., Dutrizac, J., & Gertsman, V. (2008). Synthesis and phase transformations involving scorodite, ferric arsenate and arsenical ferrihydrite: Implications for arsenic mobility. *Geochimica et Cosmochimica Acta, 72*, 2649–2672.

Paktunc, D., Foster, A., Heald, S., & Laflamme, G. (2004). Speciation and characterization of arsenic in gold ores and cyanidation tailings using X-ray absorption spectroscopy. *Geochimica et Cosmochimica Acta, 68*, 969–983.

Pearce, D. C., Dowling, K., & Sim, M. R. (2012). Cancer incidence and soil arsenic exposure in a historical gold mining area in Victoria, Australia: A geospatial analysis. *Journal of Exposure Science & Environmental Epidemiology, 22*, 248–257.

Peikam, E. N., & Jalali, M. (2017). Potential release of metals from tailings and soil at the Hamekasi Iron Mine. *Hamadan, Iran, Mine Water and the Environment, 36*, 180–192.

Rai, D., Yui, M., Schaef, H. T., & Kitamura, A. (2011). Thermodynamic model for $SnO_2(cr)$ and $SnO_2(am)$ solubility in the aqueous $Na^+–H^+–OH^-–Cl^-–H_2O$ System. *Journal of Solution Chemistry, 40*, 1155.

Rayment, G. E., Lyons, D. J., & Shelley, B. (2011). *Soil chemical methods - Australasia*. CSIRO Publishing.

Redwan, M., & Rammlmair, D. (2012). 'Understanding microenvironment development in mine tailings using MLA and image analysis. In M. A. T. M. Broekmans (Ed.), *Proceedings of the 10th International Congress for Applied Mineralogy (ICAM)* (pp. 589–596). Springer.

Reeves, R. D., van der Ent, A., & Baker, A. J. M. (2018). *Global distribution and ecology of hyperaccumulator plants*. In A. Van der Ent, G. Echevarria, A. J. M. Baker, & J. L. Morel (Eds.), *Agromining: farming for metals: extracting unconventional resources using plants* (pp. 75–92). Springer International Publishing.

Rimstidt, J. D., Chermak, J. A., & Gagen, P. M. (1994). *Rates of reaction of galena, sphalerite, chalcopyrite, and arsenopyrite with Fe(III) in acidic solutions, Environmental geochemistry of sulfide oxidation* (pp. 2–13). American Chemical Society.

Rodríguez-Hernández, A., Lázaro, I., Razo, I., & Briones-Gallardo, R. (2021). Geochemical and mineralogical characterization of stream sediments impacted by mine wastes containing arsenic, cadmium and lead in North-Central Mexico. *Journal of Geochemical Exploration, 221*, 106707.

Romero, F. M., Canet, C., Alfonso, P., Zambrana, R. N., & Soto, N. (2014). The role of cassiterite controlling arsenic mobility in an abandoned stanniferous tailings impoundment at Llallagua. *Bolivia, Science of the Total Environment, 481*, 100–107.

Rüdel, H. (2003). Case study: Bioavailability of tin and tin compounds. *Ecotoxicology and Environmental Safety, 56*, 180–189.

Sanchez-Palacios, J. T., Doronila, A. I., Baker, A. J. M., & Woodrow, I. E. (2013). Performance of *Eucalyptus* species on capped arsenic-rich gold mine tailings in the Victorian Goldfields, Australia. In M. Tibbett, A. B. Fourie, & C. Digby (Eds.), *Eighth International Seminar*

on Mine Closure (pp. 331–343). Australian Centre for Geomechanics.

Sharma, V. K., & Sohn, M. (2009). Aquatic arsenic: toxicity, speciation, transformations, and remediation. *Environment International, 35*, 743–759.

Sidenko, N. V., Khozhina, E. I., & Sherriff, B. L. (2007). The cycling of Ni, Zn, Cu in the system "mine tailings–ground water–plants": a case study. *Applied Geochemistry, 22*, 30–52.

Smith, E., Naidu, R., Weber, J., & Juhasz, A. L. (2008). The impact of sequestration on the bioaccessibility of arsenic in long-term contaminated soils. *Chemosphere, 71*, 773–780.

Sutherland, R. A. (2000). Bed sediment-associated trace metals in an urban stream. *Oahu, Hawaii, Environmental Geology, 39*, 611–627.

Tang, X.-Y., Zhu, Y.-G., Shan, X.-Q., McLaren, R., & Duan, J. (2007). The ageing effect on the bioaccessibility and fractionation of arsenic in soils from China. *Chemosphere, 66*, 1183–1190.

Telford, K., Maher, W., Krikowa, F., Foster, S., Ellwood, M. J., Ashley, P. M., Lockwood, P. V., & Wilson, S. C. (2009). Bioaccumulation of antimony and arsenic in a highly contaminated stream adjacent to the Hillgrove Mine. *NSW, Australia, Environmental Chemistry, 6*, 133–143.

Unger, C., Lechner, A., Glenn, V., Edraki, M., & Mulligan, D. (2012). *Mapping and prioritising rehabilitation of abandoned mines in Australia*. Life of Mine Conference.

Vaughan, D. J. (2006). Sulfide mineralogy and geochemistry: Introduction and overview. *Reviews in Mineralogy and Geochemistry, 61*, 1–5.

Vaughan, D. J., & Corkhill, C. L. (2017). Mineralogy of sulfides. *Elements, 13*, 81–87.

Wang, Y., Kanipayor, R., & Brindle, I. D. (2014). Rapid high-performance sample digestion for ICP determination by ColdBlock™ digestion: part 1 environmental samples. *Journal of Analytical Atomic Spectrometry, 29*, 162–168.

Wenzel, W. W. (2013). *Arsenic*. In B. J. Alloway (Ed.), *Heavy metals in soils: Trace metals and metalloids in soils and their bioavailability* (pp. 241–282). Springer.

Werner, T. T., Bach, P. M., Yellishetty, M., Amirpoorsaeed, F., Walsh, S., Miller, A., Roach, M., Schnapp, A., Solly, P., Tan, Y., Lewis, C., Hudson, E., Heberling, K., Richards, T., Chia, H. C., Truong, M., Gupta, T., & Wu, X. (2020). A geospatial database for effective mine rehabilitation in Australia. *Minerals, 10*, 745.

White, K. D., & Tittlebaum, M. E. (1985). Metal distribution and contamination in sediments. *Journal of Environmental Engineering, 111*, 161–175.

Yucel, D. S., & Baba, A. (2016). Prediction of acid mine drainage generation potential of various lithologies using static tests: Etili coal mine (NW Turkey) as a case study. *Environmental Monitoring and Assessment, 188*, 473.

Zhao, F. J., Ma, J. F., Meharg, A. A., & McGrath, S. P. (2009). Arsenic uptake and metabolism in plants. *New Phytologist, 181*, 777–794.